

Registration made easy – standalone orthopedic navigation with HoloLens

Florentin Liebmann^{1,2}, Simon Roner^{1,3}, Marco von Atzigen^{1,2}, Florian Wanivenhaus³, Caroline Neuhaus, José Spirig³, Davide Scaramuzza^{5,6}, Reto Sutter⁷, Jess Snedeker^{2,3}, Mazda Farshad³, and Philipp Fürnstahl¹

¹ Computer Assisted Research & Development, Balgrist University Hospital

² Laboratory for Orthopaedic Biomechanics, ETH Zurich

³ Orthopaedic Department, Balgrist University Hospital, University of Zurich

⁵ Department of Informatics, University of Zurich

⁶ Department of Neuroinformatics, University of Zurich and ETH Zurich

⁷ Radiology Department, Balgrist University Hospital, University of Zurich

Abstract

In surgical navigation, finding correspondence between preoperative plan and intraoperative anatomy, the so-called registration task, is imperative. One promising approach is to intraoperatively digitize anatomy and register it with the preoperative plan. State-of-the-art commercial navigation systems implement such approaches for pedicle screw placement in spinal fusion surgery. Although these systems improve surgical accuracy, they are not gold standard in clinical practice. Besides economical reasons, this may be due to their difficult integration into clinical workflows and unintuitive navigation feedback. Augmented Reality has the potential to overcome these limitations. Consequently, we propose a surgical navigation approach comprising intraoperative surface digitization for registration and intuitive holographic navigation for pedicle screw placement that runs entirely on the Microsoft HoloLens. Preliminary results from phantom experiments suggest that the method may meet clinical accuracy requirements.

1. Introduction

Finding correspondence between preoperative surgical plan and intraoperative anatomy is one of the core tasks in surgical navigation. This process is referred to as registration. Markelj *et al.* [13] give a good overview on clinical imaging modalities and the resulting registration possibilities. Preoperative data are 3D computed tomography (CT) or magnetic resonance images. In orthopedic surgery, common 2D imaging modalities are ultrasound (US), flu-

oroscopy or optical images. Cone-beam CT (CBCT), US and reconstruction with optical systems are 3D data sources. Consequently, intraoperative registrations are either 3D/2D or 3D/3D. 3D/3D is further subdivided into *image-to-image* and *image-to-patient* (when reconstruction with optical systems is employed).

In terms of 3D/2D registration, the most widely used approach involves digitally reconstructed radiographs (DRR), i.e. simulated 2D views generated from preoperative 3D data. The DRR are compared to intraoperative 2D fluoroscopic images using a similarity measure which can be optimized in an iterative fashion. However, surgical tools, implants and resected soft tissue which are usually not present in preoperative images make this approach challenging [6]. DRR generation is computationally expensive and a balance between robustness and computational cost has to be found [14]. Moreover, a calibrated intraoperative setup is required.

Apart from a technical point of view, any intraoperative imaging that implies radiation exposure for patient and OR personnel is considered critically (e.g. [16]). This adversely affects the use of intraoperative fluoroscopy and especially CBCT. 2D and 3D US are radiation-free alternatives. Nevertheless, they are not well-suited for open surgery due to their reliance on a transportation medium (e.g. [30]).

Summarizing above findings, radiation-free 3D/3D image-to-patient registration can be considered most promising. An exemplary method following this approach is *Surface Matching*, in which a 3D reconstruction of the visible anatomy is achieved by sampling bone surface with a tracked pointer. It is implemented in state-of-the-art commercial navigation systems and is well-known for pedicle

screw placement in spinal fusion surgery [23, 18, 5]. Although such systems increase accuracy, they are not established as the clinical gold standard [1]. Besides high costs for acquisition and maintenance, the main reason may be that they cannot be integrated into clinical practice without effort and hinder seamless workflows (e.g. line of sight issues) [27]. Furthermore, anatomical 3D models and navigation feedback are not superimposed in situ, but visualized on peripheral 2D monitors which makes it hard to comprehend the underlying 3D space in an intuitive way [22].

Augmented Reality (AR) has the potential to overcome these limitations. It has been considered interesting for medical applications for more than a decade [25, 17], but only recent technological advancement allows for the development of computationally powerful, off-the-shelf optical see-through head mounted-displays [21]. We proposed a radiation-free surgical navigation approach comprising intraoperative manual surface digitization for registration and intuitive holographic navigation for pedicle screw placement that runs entirely on the Microsoft HoloLens [12]. The methodology of our approach and a pre-clinical evaluation are presented together with another in-house HoloLens application related to spinal fusion surgery [29].

2. Methods

The presented method consists of two main components: intraoperative registration and surgical navigation. Both rely on 6DoF marker tracking.

2.1. Marker tracking and pose estimation

Marker tracking was implemented employing the two front-facing of the four environment tracking cameras that are accessible via Research Mode [15]. Commercial, sterile fiducial markers (Clear Guide Medical, Baltimore MD, USA) were used. Their patterns originate from the AprilTags library [19, 28]. We refer to the official terminology of the HoloLens coordinate systems to describe the process: App-specified Coordinate System (ASCS), Camera Coordinate System (CCS), 3D Camera View Space (CVS) and 2D Camera Projection Space (CPS). CVS and CPS of the left and right camera are termed CVSL/CVSR and CPSL/CPSR, respectively. An exemplary transformation from CPS to CVS is denoted as T_{CPS}^{CVS} .

For each pair of images (left and right) with a detectable marker, its pose is derived as follows. Initial estimate values C_1^L, \dots, C_4^L and C_1^R, \dots, C_4^R of the four corners of the marker are detected in both images using the ArUco library [7, 8, 24]. Due to the low resolution (480×640 pixels) of the environmental cameras, each C_i is passed to a dedicated Kalman filter with a constant velocity model [11, 3].

The filtered corner estimates are transformed to CPS and extended by one dimension (unit plane: $z = 1$) such that they can be expressed in CVS and further transformed to

CCS. To perform triangulation, directional vectors \vec{d}_i^L and \vec{d}_i^R between each $T_{CPSL}^{CCS}C_i^L$ and $T_{CPSR}^{CCS}C_i^R$ and their respective camera centers are formed. Triangulation can be completed by finding the closest point $\min(\vec{d}_i^L, \vec{d}_i^R)$ between each pair of directional vectors.

Given the new 3D estimates $\min(\vec{d}_i^L, \vec{d}_i^R)$, the 6DoF marker pose is derived by incorporating prior knowledge about the marker geometry. As the true 3D position gt_i of each corner point with respect to the marker center is known, the pose estimation problem can be reduced to finding a rigid transformation between the point pairs $\min(\vec{d}_i^L, \vec{d}_i^R)$ and gt_i in a least-square sense. The transformation results from applying the absolute orientation [10].

2.2. Registration

The idea of our surface digitization approach is to establish correspondence between pre- and intraoperative anatomy without using intraoperative imaging.

For each vertebra, a sparse point cloud of relevant bone surface regions is collected by the surgeon. A custom-made pointing device (PD, Figure 1a) is used for surface acquisition. The PD consists of a notch, a handle and a tip. The tip is tapered in a way such that points can be reached at different angles without introducing an offset. The notch can be mounted with a previously described marker (Section 2.1). The known geometry of the PD makes it straightforward to extrapolate from marker pose to tip position.

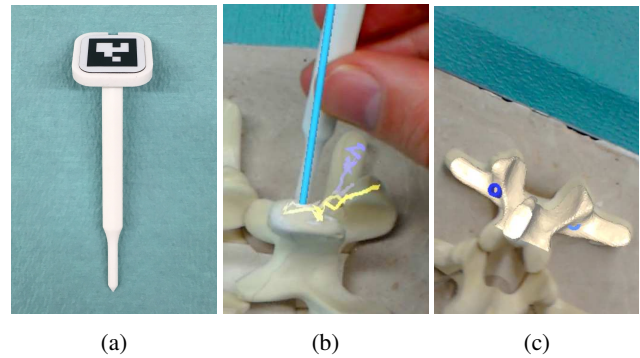


Figure 1: a) Custom-made pointing device. b) Augmented view of the surgeon during surface sampling. c) Vertebra overlay after registration (insertion points denoted in blue).

Reprinted by permission from RightsLink: Springer International Journal of Computer Assisted Radiology and Surgery [12]. © CARS (2019), advance online publication, 15 April 2019 (doi: 10.1007/s11548-019-01973-7.IICARS.)

After application startup, the surgeon is asked to sample accessible surface regions of the vertebra in a specific pattern which was trained previously. To do so, the PD is moved along the anatomy while pressing down the button of the HoloLens clicker. The 3D tip position is recorded, as long as the button remains pressed. Sampled areas are visualized by a thin line connecting consecutively collected

points (Figure 1b). Once the button is released, a voice command can be used to indicate whether the just collected region should be saved (“save”) or discarded (“delete”). Only the saved points are used for registration. When sufficient points have been sampled, a double click starts registration.

The intraoperatively collected point cloud pc_{intra} is registered to the point cloud pc_{pre} representing the points of the 3D model of the preoperative vertebra. In a preprocessing step, pc_{pre} is trimmed by removing points which can definitely not be reached with the PD in a surgery.

The automated registration process comprises three steps: coarse registration, iterative closest point (ICP) based fine registration [2] and result selection. Coarse registration is achieved by identifying three corresponding extreme points in each of the point clouds. To this end, a principle component analysis (PCA) [20], implemented in ALGLIB (ALGLIB Project, Nizhny Novgorod, Russia), is performed on pc_{intra} , yielding the respective principle axes pa_1^{intra} , pa_2^{intra} and pa_3^{intra} ordered by decreasing magnitude. The three extreme points e_1^{intra} , e_2^{intra} and e_3^{intra} are determined using the dot product (Figures 2a and 2b):

$$\begin{aligned} e_1^{intra} &= \max(pa_1^{intra} \cdot p_i), \forall p_i \in pc_{intra} \\ e_2^{intra} &= \min(pa_1^{intra} \cdot p_i), \forall p_i \in pc_{intra} \\ e_3^{intra} &= \max(|pa_2^{intra} \cdot p_i|), \forall p_i \in pc_{intra} \end{aligned} \quad (1)$$

Correspondingly, the extreme points e_1^{pre} , e_2^{pre} and e_3^{pre} are calculated. Due to vertebra symmetry along pa_1 , two possible coarse registration configurations must be evaluated (Figures 2a and 2b) and considered for the fine registration by applying absolute orientation [10] to both point pair sets:

$$\begin{aligned} \{(e_1^{intra}, e_1^{pre})\}, \{(e_2^{intra}, e_2^{pre})\}, \{(e_3^{intra}, e_3^{pre})\} \\ \{(e_1^{intra}, e_2^{pre})\}, \{(e_2^{intra}, e_1^{pre})\}, \{(e_3^{intra}, e_3^{pre})\} \end{aligned} \quad (2)$$

Afterwards, fine registration is performed using ICP on both configurations and the one with the smaller final RMSE is selected (Figure 2c). The result is shown to the surgeon by superimposing the preoperative 3D model with the intraoperative anatomy (Figure 1c) and is verified visually.

2.3. Clinical application

In spinal fusion surgery, screws are inserted into the pedicles of pathological spine levels. The screw heads are then rigidly connected to each other by means of a rod [9]. Accurate screw insertion is crucial to avoid harming vital structure as nerves. Bending said rod can be complicated in complex deformity cases. Commonly, a wire is used in situ to form a template. The rod is then bent ex situ according to the wire using dedicated tools. This can be tedious process. To this end, we propose navigation methods for screw insertion and rod bending. Please note that in our study K-Wires instead of actual pedicle screws were inserted.

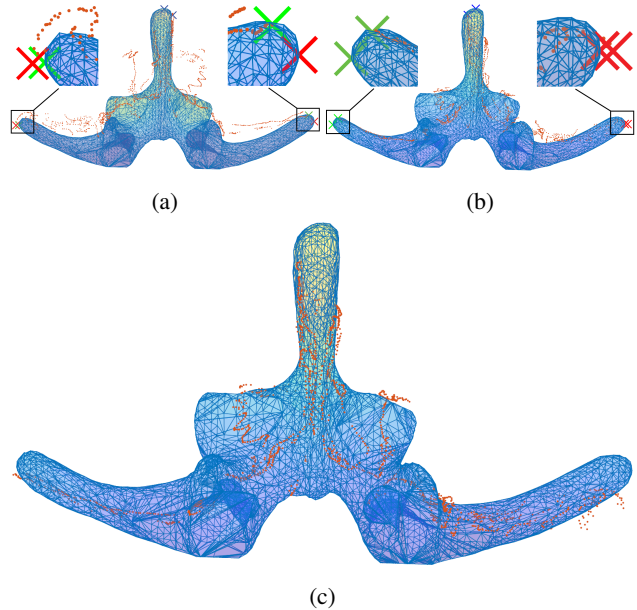


Figure 2: pc_{pre} denotes the points of the 3D model. pc_{intra} is shown in orange. The red, green and blue crosses in a) and b) represent the respective extreme points used for coarse alignment. a) Incorrect coarse alignment. b) Correct coarse alignment. c) The fine alignment resulting from b).

Reprinted by permission from RightsLink: Springer International Journal of Computer Assisted Radiology and Surgery [12]. © CARS (2019), advance online publication, 15 April 2019 (doi: 10.1007/s11548-019-01973-7.IICARS.)

Screw navigation relies on a trackable (Section 2.1) custom-made surgical navigation tool (NT, Figures 3a and 3c). Handle and sleeve are designed such that they allow holding the ND with one hand, while inserting a K-wire with the other (Figure 3a). Navigation can be started after

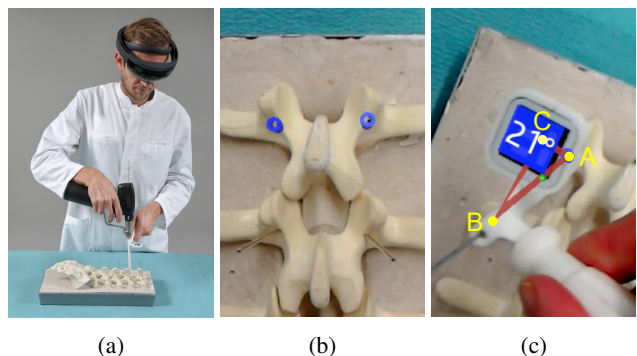


Figure 3: a) A surgeon uses the custom-made surgical navigation tool. b) Entry point overlay (blue) in the beginning of the navigation. c) Augmented view of the surgeon during navigation (except yellow points).

Reprinted by permission from RightsLink: Springer International Journal of Computer Assisted Radiology and Surgery [12]. © CARS (2019), advance online publication, 15 April 2019 (doi: 10.1007/s11548-019-01973-7.IICARS.)

successful registration (Section 2.2). First, the screw entry points are shown (Figure 3b). The pointed K-wire tip is pierced into the bone at the targeted position, purely relying on holographic visualization. The K-wire tip does not slide away and the surgeon can start to navigate towards the desired trajectory. Thereby, holographic feedback comprises two parts of information (Figure 3c). First, the 3D angle between current and targeted trajectory is displayed. Second, a triangle is rendered between three virtual points: the screw entry point (A), a point lying on the current trajectory of the NT (B) and one lying on the targeted screw trajectory (C). This way, the surgeon is given an intuitive feedback about trajectory deviation in 3D space.

Rod bending navigation is based on calculating and displaying a holographic template of the optimal rod shape. It does not require registration with the anatomy, but the same tracked PD (Figure 1a) is employed to capture the head position for each screw. From these 3D points, a centripetal Catmull-Rom spline is calculated and the rod length is estimated (Figure 4a). A Catmull-Rom spline is a piecewise function that passes through its defining points [4], i.e. the stored screw head positions. We use the centripetal parametrization as iof self-intersections and cusps within curve segments [31]. Finally, the newly created spline is moved away from the patient and the rod is bent according to the holographic template (Figure 4b).

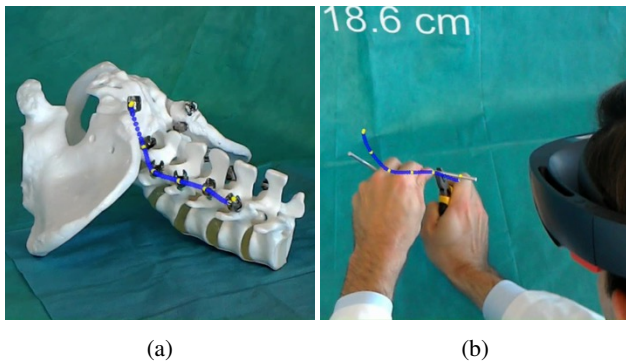


Figure 4: a) The rod template. b) Shared experience capture of a surgeon bending a rod according to the template. Please note that both images originate from [29].

2.4. Pre-clinical evaluation

Our method for screw navigation was evaluated on two phantoms of the lower lumbar spine that were molded into a plastic tub to mimic clinical accessibility of vertebra surfaces (e.g. Figure 3b). Screw trajectories were planned preoperatively (Figure 5a). Each vertebra was registered individually and two K-wires (left and right) representing the pedicle screws were inserted, solely relying on AR navigation. After execution, postoperative 3D models of vertebrae

and inserted K-Wires were generated from CT scans and aligned to the preoperative plan. For each K-wire, trajectory and entry point were quantified. The trajectory was defined by aligning a generic cylindrical object to the segmented K-wire (Figure 5b). The entry point was defined as the first point along the trajectory intersecting with the preoperative 3D model (Figure 5c). Primary results were the 3D angle between planned and executed trajectories as well as the 3D distance between planned and executed entry points. Secondary results for each vertebra included registration error, surface digitization time and the number of sampled points.

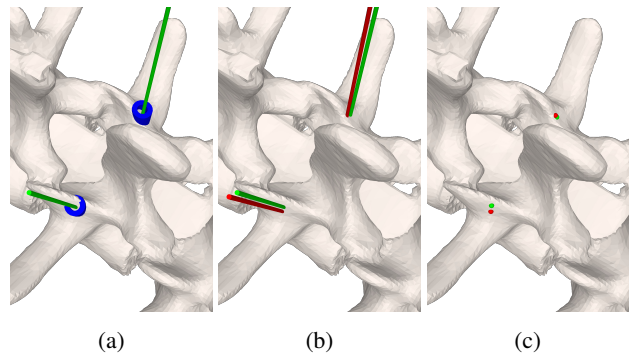


Figure 5: a) Planned trajectories (green) and entry points (blue). b) Planned trajectories (green) and red cylinder representing postoperatively segmented K-wires. c) Planned (green) and postoperatively quantified entry points (red).

Reprinted by permission from RightsLink: Springer International Journal of Computer Assisted Radiology and Surgery [12]. © CARS (2019), advance online publication, 15 April 2019 (doi: 10.1007/s11548-019-01973-7.IJCARS.)

The rod bending navigation was evaluated on an instrumented phantom of the lumbar spine (Figure 4a) by comparison with the standard trial-and-error technique. For each group, a total of six rods were bent by three surgeons. The time for bending and insertion, the number of rod-rebending maneuvers and the rod length accuracy were recorded.

3. Results and discussion

Results of our screw navigation experiments are listed in Table 1. The mean registration RMSE (1.62 mm) and time (125 s) are comparable to state-of-the-art systems (e.g. 0.9 mm and 117 s in Nottmeier and Crosby [18]). The accuracy is promising and suggests that the method has the potential for clinical use.

All of the rod bending navigation results were in favor of the AR group, with time exposure (374 vs. 465 s) and rod length (15/18 vs 4/18 correct) showing significant differences. Clinical trials are imminent.

The screw navigation method has limitations. Our experimental setup was simplified by rigidly attaching the phantoms to a table. This obviated motion compensation, but

Result	Mean	SD	min.	max.
Trajectory err. (°)	3.38	1.73	1.16	6.33
Entry point err. (mm)	2.77	1.46	0.71	7.20
Reg. RMSE (mm)	1.62	0.26	1.14	2.02
Digitization time (s)	125	27	91	185
# points collected	1983	404	1268	2744

Table 1: Results of screw navigation experiments.

holograms are prone to drift after placement [26]. This may have negatively influenced our results, although the surgeon tried to minimize head movement during the experiments. On another note, the use of Research Mode sensors for stereo vision negatively affects application stability as they are an essential part of the HoloLens’ built-in SLAM. It is assumed that all such capabilities will perform even better in upcoming releases.

Our results encourage 3D/3D image-to-patient registration. For future work, we plan to employ RGB-D sources, such as Azure Kinect DK, promoting an automated process.

References

- [1] Sebastian Andress, Alex Johson, Mathias Unberath, Alexander Winkler, Kevin Yu, Javad Fotouhi, Simon Weidert, Greg Osgood, and Nassir Navab. on-the-fly augmented reality for orthopaedic surgery using a multi-modal fiducial. In *Medical Imaging 2018: Image-Guided Procedures, Robotic Interventions, and Modeling*, volume 10576, page 105760H. International Society for Optics and Photonics, 2018. [2](#)
- [2] Paul J Besl and Neil D McKay. Method for registration of 3-d shapes. In *Sensor Fusion IV: Control Paradigms and Data Structures*, volume 1611, pages 586–607. International Society for Optics and Photonics, 1992. [3](#)
- [3] Gary Bradski and Adrian Kaehler. *Opencv. Dr. Dobbs journal of software tools*, 3, 2000. [2](#)
- [4] Edwin Catmull and Raphael Rom. A class of local interpolating splines. In *Computer aided geometric design*, pages 317–326. Elsevier, 1974. [4](#)
- [5] CY Fan Chiang, Tsung-Ting Tsai, Lih-Huei Chen, Po-Liang Lai, Tsai-Sheng Fu, Chi-Chien Niu, and Wen-Jer Chen. Computed tomography-based navigation-assisted pedicle screw insertion for thoracic and lumbar spine fractures. *Chang Gung Med J*, 35(4):332–8, 2012. [1](#)
- [6] T De Silva, A Uneri, MD Ketcha, S Reaungamornrat, G Kleinszig, S Vogt, Nafi Aygun, SF Lo, JP Wolinsky, and JH Siewerdsen. 3d–2d image registration for target localization in spine surgery: investigation of similarity metrics providing robustness to content mismatch. *Physics in Medicine & Biology*, 61(8):3009, 2016. [1](#)
- [7] Sergio Garrido-Jurado, Rafael Muñoz-Salinas, Francisco José Madrid-Cuevas, and Manuel Jesús Marín-Jiménez. Automatic generation and detection of highly reliable fiducial markers under occlusion. *Pattern Recognition*, 47(6):2280–2292, 2014. [2](#)
- [8] Sergio Garrido-Jurado, Rafael Muñoz-Salinas, Francisco José Madrid-Cuevas, and Rafael Medina-Carnicer. Generation of fiducial marker dictionaries using mixed integer linear programming. *Pattern Recognition*, 51:481–491, 2016. [2](#)
- [9] Jürgen G Harms and Dezsö Jeszenszky. Die posteriore, lumbale, interkorporelle fusion in unilateraler transforaminaler technik. *Operative Orthopädie und Traumatologie*, 10(2):90–102, 1998. [3](#)
- [10] Berthold KP Horn. Closed-form solution of absolute orientation using unit quaternions. *JOSA A*, 4(4):629–642, 1987. [2, 3](#)
- [11] Rudolph Emil Kalman. A new approach to linear filtering and prediction problems. *Journal of basic Engineering*, 82(1):35–45, 1960. [2](#)
- [12] Florentin Liebmann, Simon Roner, Marco von Atzigen, Davide Scaramuzza, Reto Sutter, Jess Snedeker, Mazda Farshad, and Philipp Fürnstahl. Pedicle screw navigation using surface digitization on the microsoft hololens. *International journal of computer assisted radiology and surgery*, pages 1–9, 2019. [2, 3, 4](#)
- [13] Primoz Markelj, Dejan Tomažević, Bostjan Likar, and Franjo Pernuš. A review of 3d/2d registration methods for image-guided interventions. *Medical image analysis*, 16(3):642–661, 2012. [1](#)
- [14] Shun Miao, Sebastien Piat, Peter Fischer, Ahmet Tuysuzoglu, Philip Mewes, Tommaso Mansi, and Rui Liao. Dilated fcn for multi-agent 2d/3d medical image registration. In *Thirty-Second AAAI Conference on Artificial Intelligence*, 2018. [1](#)
- [15] Microsoft. HoloLens research mode, 2018. [2](#)
- [16] Ankur S Narain, Fady Y Hijji, Kelly H Yom, Krishna T Kudaravalli, Brittany E Haws, and Kern Singh. Radiation exposure and reduction in the operating room: Perspectives and future directions in spine surgery. *World journal of orthopedics*, 8(7):524, 2017. [1](#)
- [17] Nassir Navab, Tobias Blum, Lejing Wang, Asli Okur, and Thomas Wendler. First deployments of augmented reality in operating rooms. *Computer*, 45(7):48–55, 2012. [2](#)
- [18] Eric W Nottmeier and Tracey L Crosby. Timing of paired points and surface matching registration in three-dimensional (3d) image-guided spinal surgery. *Clinical Spine Surgery*, 20(4):268–270, 2007. [1, 4](#)
- [19] Edwin Olson. Apriltag: A robust and flexible visual fiducial system. In *Robotics and Automation (ICRA), 2011 IEEE International Conference on*, pages 3400–3407. IEEE, 2011. [2](#)
- [20] Karl Pearson. Liii. on lines and planes of closest fit to systems of points in space. *The London, Edinburgh, and Dublin Philosophical Magazine and Journal of Science*, 2(11):559–572, 1901. [3](#)
- [21] Long Qian, Alexander Barthel, Alex Johnson, Greg Osgood, Peter Kazanzides, Nassir Navab, and Bernhard Fuerst. Comparison of optical see-through head-mounted displays for surgical interventions with object-anchored 2d-display.

International journal of computer assisted radiology and surgery, 12(6):901–910, 2017. 2

- [22] Long Qian, Mathias Unberath, Kevin Yu, Bernhard Fuerst, Alex Johnson, Nassir Navab, and Greg Osgood. Towards virtual monitors for image guided interventions-real-time streaming to optical see-through head-mounted displays. *arXiv preprint arXiv:1710.00808*, 2017. 2
- [23] Marcus Richter, Balkan Cakir, and René Schmidt. Cervical pedicle screws: conventional versus computer-assisted placement of cannulated screws. *Spine*, 30(20):2280–2287, 2005. 1
- [24] Francisco J Romero-Ramirez, Rafael Muñoz-Salinas, and Rafael Medina-Carnicer. Speeded up detection of squared fiducial markers. *Image and Vision Computing*, 2018. 2
- [25] Tobias Sielhorst, Marco Feuerstein, and Nassir Navab. Advanced medical displays: A literature review of augmented reality. *Journal of Display Technology*, 4(4):451–467, 2008. 2
- [26] Reid Vassallo, Adam Rankin, Elvis CS Chen, and Terry M Peters. Hologram stability evaluation for microsoft hololens. In *Medical Imaging 2017: Image Perception, Observer Performance, and Technology Assessment*, volume 10136, page 1013614. International Society for Optics and Photonics, 2017. 5
- [27] Jan Victor and Davy Hoste. Image-based computer-assisted total knee arthroplasty leads to lower variability in coronal alignment. *Clinical Orthopaedics and Related Research®*, 428:131–139, 2004. 2
- [28] John Wang and Edwin Olson. Apriltag 2: Efficient and robust fiducial detection. In *IROS*, pages 4193–4198, 2016. 2
- [29] Florian Wanivenhaus, Caroline Neuhaus, Florentin Liebmann, Simon Roner, José M Spirig, and Mazda Farshad. Augmented reality-assisted rod bending in spinal surgery. *The Spine Journal*, 19(10):1687–1689, 2019. 2, 4
- [30] Charles XB Yan, Benoît Goulet, Donatella Tampieri, and D Louis Collins. Ultrasound-ct registration of vertebrae without reconstruction. *International journal of computer assisted radiology and surgery*, 7(6):901–909, 2012. 1
- [31] Cem Yuksel, Scott Schaefer, and John Keyser. On the parameterization of catmull-rom curves. In *2009 SIAM/ACM Joint Conference on Geometric and Physical Modeling*, pages 47–53. ACM, 2009. 4